

Simulated Emission Depletion microscopy to study amyloid fibril formation

Pierre Mahou^a, Nathan Curry^a, Dorothea Pinotsi^a Gabriele Kaminski Schierle^a & Clemens F. Kaminski^a

^aDepartment of Chemical Engineering and Biotechnology, University of Cambridge, United Kingdom.

pm538@cam.ac.uk, cfk23@cam.ac.uk

ABSTRACT

Aggregation of misfolded proteins is a characteristic hallmark of many neurodegenerative disorders, such as Parkinson's, Alzheimer's and Huntington's diseases. The ability to observe these aggregation processes and the corresponding structures formed *in vitro* or *in situ* is therefore a key requirement to understand the molecular mechanisms of these diseases. We report here on the implementation and application of Stimulated Emission Depletion (STED) microscopy to visualize the formation of amyloid fibrils *in vitro*.

Keywords: Super resolution microscopy, Stimulated Emission Depletion microscopy, amyloid fibrils.

1. INTRODUCTION

Neurodegenerative disorders include more than 600 pathologies afflicting the nervous system. The most common pathologies are: Alzheimer's disease, Parkinson's disease, Huntington's disease and amyotrophic lateral sclerosis. These disorders are often associated with a progressive loss of neurons structure and function starting from different parts of the brain before spreading to other regions. One of the main features of these disorders is that they exhibit similarities that relate them to one another at the molecular level: lesions found in the brain of patients have been associated with fibrillar aggregates of proteins such as: amyloid β , α -synuclein, tau or huntingtin^{1,2}. Under certain physiological conditions these proteins tend to misfold and aggregate, forming the so-called amyloid fibrils with remarkably common structures and morphologies. Amyloid fibrils consist of individual beta-sheet-rich protofibrils, which are twisted around a common axis to form fibre-like structures with diameters in the range of 2 to 15 nm and with lengths that can reach up to several micrometres³. Understanding the fundamental mechanism behind the formation of these fibrillar aggregates is therefore a key challenge of current biophysical and life science research.

Previous studies using nuclear magnetic resonance (NMR), electron microscopy (EM) or atomic force microscopy (AFM) have extensively characterized the structural properties of a broad range of amyloid fibrils⁴⁻⁶. These techniques have been invaluable to investigate mature amyloid fibrils or intermediates isolated from the aggregation process *in vitro*. On the other hand, conventional microscopy methods, which compared to the aforementioned techniques, can be applied to study aggregation kinetics directly and non-invasively, have proven valuable in this context. For example, Thioflavin T based-assays are currently the bench-mark for the characterization amyloid fibril kinetics⁷⁻⁹. However, since the characteristic length scale of the protein assemblies is two orders of magnitude smaller than the spatial resolution of conventional optical microscopes such approaches are limited to ensemble measurements. This is currently limiting as it has been shown that amyloid fibrils exhibit inhomogeneous growth kinetics over extended periods of time¹⁰. This suggests that there is a compelling need for simple biophysical methods with intermediate resolving power enabling to map and characterize the kinetics of amyloid fibrils directly and non-invasively^{10,11}. In this context, we report here on the implementation and application of a Stimulated Emission Depletion (STED) microscope to visualize amyloid fibrils and which, in the future, will permit the extraction of quantitative parameters on fibril growth kinetics.

2. IMPLEMENTATION OF STED MICROSCOPY

2.1 Principle

Stimulated Emission Depletion (STED) microscopy, introduced in 1994 by Hell and Wichman¹², is one of the super-resolution techniques¹³⁻¹⁵ breaking the diffraction limit. STED microscopy, was first implemented in the confocal geometry¹⁶ to improve the resolution along two or three dimensions¹⁷ but has also been extended to other illumination and detection geometries such as to orthogonal^{18,19} or to wide-field-based geometries²⁰⁻²².

In confocal laser scanning microscopy, the samples labelled by a fluorescent protein or a dye, such as ATTO 647N, are mapped by raster scanning a focused laser beam across the region of interest (Figure 1a). For each position of the excitation spot (centered at $\lambda = 640$ nm) the red fluorescence generated by the emitting fluorophores is collected in the range of 650-720nm and an image is reconstructed digitally pixel by pixel. Generally, due to the diffraction of light for each pixel the fluorescence is collected over a volume which lateral and axial extensions at full width half maximum are approximately given by the following expressions²³:

$$\delta_{XY} \approx 0.5 \times \lambda / NA \quad (1)$$

$$\delta_Z \approx 0.9 \times \lambda / (n - \sqrt{n^2 - NA^2}), \quad (2)$$

where NA is the numerical aperture of the microscope objective lens and n the refractive index of the immersion liquid. This sets the axial and lateral resolution to about 230 nm and 590 nm respectively for a lens with $NA = 1.4$ and means that each detail in the sample finer than these typical length scales is "lost" in the final image (Figure 1a). To break this resolution limit, STED microscopy uses stimulated emission depletion to prevent fluorescence emission from the molecules on the outer part of the excitation volume. In the two-dimensional case, this is generally achieved by superimposing a doughnut-shaped beam to the excitation beam. Given that its central wavelength lies outside the detection band, the molecules undergoing spontaneous emission can be distinguished from the molecules undergoing stimulated emission. By saturating the depletion, fluorescence originates only from a small volume near the optical axis and the effective lateral resolution depends on the depletion intensity I_{STED} , the stimulated emission cross section σ , and the fluorescence lifetime τ_{fl} of the dye as follows:

$$\delta_{XY} = \frac{0.5 \times \lambda / NA}{\sqrt{1 + \sigma \tau_{fl} \times I_{STED}}} \quad (3)$$

In theory, the resolution is unbounded, but in practice it is limited to 30–80 nm by the photostability of the probes and the signal to noise ratio. Although STED microscopy has been implemented using continuous wave excitation²⁴, in the present study we report on the implementation of the technique using a pulsed laser and present how a commercial confocal microscope can be converted into a STED microscope and then used to map the aggregation of misfolded proteins.

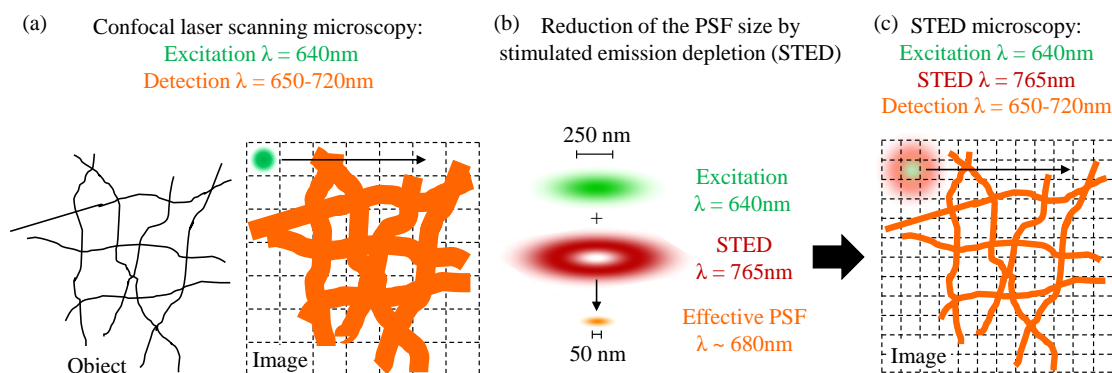


Figure 1. Principle of confocal laser scanning microscopy and Stimulated Emission Depletion microscopy.

2.2 Optical Set up

The optical set up of our STED microscope is depicted in Figure 2. It has been optimized for red fluorescent dyes or proteins, such as ATTO 647N, STAR 635 and TagRFP^{25,26}. It comprises two synchronized pulsed trains deriving from a single titanium:sapphire laser (Ti:S, Mai Tai HP, Spectraphysics), whose specifications are listed in Table 1. The excitation and depletion pulse trains are thus temporally synchronized by design, making the use of electronic synchronization unnecessary.

Table 1. Specifications of the titanium:sapphire laser and the derived beams for fluorescence excitation and depletion.

	Ti:S	Excitation	Depletion
Central wavelength	765 nm	640 nm	765 nm
Pulse duration (τ)	100 fs	60 ps	100 ps
Repetition rate (T_{Rep})	80 MHz	80 MHz	80 MHz

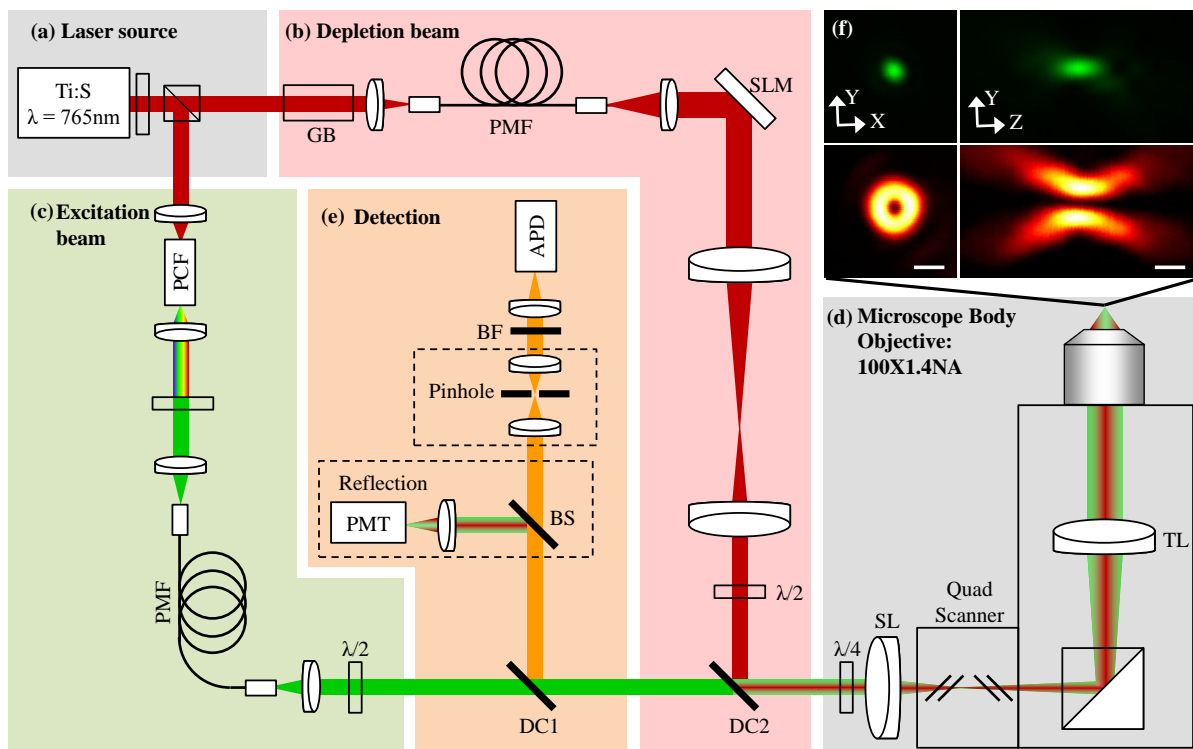


Figure 2. Schematic of the home-built STED microscope. (a-c) The excitation and depletion beam required for STED originate from a single pulsed laser centered at $\lambda = 765$ nm. (d) The excitation and depletion beams are sent to a point-scanning microscope and images are acquired by raster scanning the beams across the sample. (e) Detection module: fluorescence is collected by an avalanche photodiode before being reflected off a dichroic mirror and filtered by a bandpass filter. Alternatively, light scattered by the sample can be collected by a photomultiplier tube after reflection off a pellicle beam splitter. (f) Measurement of the excitation and depletion point spread functions using gold nanobeads. Scale bars: 500 nm.

To control the overall power of the Ti:S laser a motorized half wave plate and a polarization beam splitter are placed directly at the output of the Ti:S laser (not shown). The beam of the Ti:S laser is then split into two beams by a second pair of a motorized half wave plate and a polarization beam splitter to generate the excitation and depletion pulse trains (Figure 2(a-c)). The reflected beam is focused onto a photonic crystal fiber (FemtoWhite, NKT Photonics) to generate a white-light radiation with a spectral density of approximately 0.1mW/nm, from 500–700nm. After collimation, the

excitation pulse train is extracted from the supercontinuum source with bandpass filters and coupled into a 30 m long polarization maintaining single-mode fiber (PM630-HP, Thorlabs). The transmitted beam is then passed through a 48 cm long glass block of SF66 to minimize spectral broadening due to self-phase modulation and coupled into a 100 m long polarization maintaining single-mode fiber (PM630-HP, Thorlabs). Based on Sellmeier coefficients of fused silica the final pulse duration of the excitation and depletion beams should then be 60 and 100 ps, respectively. After collimation, the excitation and depletion beams are spatially overlapped with a dichroic mirror (T735spxr, Chroma) and sent to a commercial beam-scanning microscope (Figure 1(d-e)) provided by Abberior Instruments. The beams are focused onto the sample by a 100x/1.4 NA oil immersion objective lens (UPLSAPO 100XO, Olympus) mounted on a microscope frame (IX83, Olympus) and images are acquired by raster scanning four galvanometer mirrors (Quad scanner, Abberior Instruments). The scanners provide a true standing pattern on the back aperture of the microscope lens guaranteeing an identical depletion beam on the sample in a field of view of $80 \times 80 \mu\text{m}^2$ ²⁷. To locally quench the fluorescence generated by the excitation beam, the depletion beam is shaped into a so-called doughnut beam produced by a spatial light modulator (X10468-02, Hamamatsu)²⁸. The device is used to spatially shape the phase of the depletion beam on the back aperture of the microscope lens, thanks to two pairs of achromatic doublets imaging the spatial light modulator chip. Eventually, the fluorescence photons emerging from the sample are collected by the microscope objective lens, and after being descanned, are sent to a pinhole and an avalanche photodiode (SPCM-AQRH, Excelitas Technologies) by a dichroic mirror. Alternatively, recording of the excitation and depletion point spread functions is performed by collecting the light scattered by gold nanoparticles (Abberior) with a photomultiplier tube (H10723-20, Hamamatsu) and a pellicle beam splitter mounted on a motorized stage (Figure 2(e-f)).

2.3 STED microscope made simpler with a Spatial Light Modulator

The complexity of STED microscopes originates from two main factors. First, it requires two synchronized pulsed beams with pulse duration of approximately 100 ps, central wavelengths matching the excitation and emission spectra of the dyes but most importantly the depletion beam requires sufficient peak power to deplete efficiently the excited fluorophores. Over the past few years, new laser sources have been developed to facilitate the implementation of STED microscopes²⁹⁻³². However, STED microscopy also requires microscope objective lenses with high numerical aperture, diffraction limited beams, the appropriate depletion pattern and the precise co-alignment between the excitation and depletion beams. The use of high numerical aperture and high magnification objectives makes the last three criteria even harder to fulfil. In particular, the so-called ‘hollow’ or ‘bottle’ beams, which are used for two- or three-dimensional STED microscopy and are conventionally produced by static phase masks, are particularly sensitive to decentring and optical aberrations³³. This necessitates particular care on the alignment and on the choice of optics introduced in the beam path, such that the overall aberrations induced by the system are insignificant. In this regard, the use of a liquid crystal based spatial light modulator was proposed to simulate a conventional diffraction mask and correct for the optical aberrations of the system simultaneously^{28,30,34}. As illustrated in Figure 3(a-b) this strategy can be implemented efficiently into a commercial confocal microscope in order to obtain diffraction-limited hollow or bottle beams (data not shown) with a 100x/1.4 NA oil immersion objective lens. We note, although this configuration is imperfect as it only corrects for the optical aberrations of the depletion beam it is in practice effective since the performance of a STED microscope is often limited by the quality of the depletion beam^{33,35}.

Furthermore, in STED microscopy misalignments between the excitation and depletion beams affect the microscope performance. These misalignments derive from several causes. First, since the central wavelengths of the excitation and depletion beam lay in the visible and near-infrared spectrum, respectively, chromatic aberrations induced by the microscope objective lens lead to mismatch mainly along the optical axis. Secondly, imperfect alignment between the two beams before the microscope leads to a mismatch perpendicular to the optical axis, as they are exacerbated by the microscope objective lens which magnification is in the range of 60-100. In this regard, the use of a spatial light modulator considerably simplifies the operation of STED microscopes, as phase patterns affecting independently the lateral or axial shift of the depletion beam, corresponding to Zernike modes and called defocus tip and tilt, respectively can be simulated and added to the pre-existing pattern. As illustrated in Figure 3(c and d) this enables a computer-control of the beam alignment at the focus of a 100x/1.4 NA oil immersion objective lens and therefore permits the automatic co-alignment of the beams. This method simplifies the operation of a STED microscope, in particular since effects of thermal drift during a day of operation are not negligible.

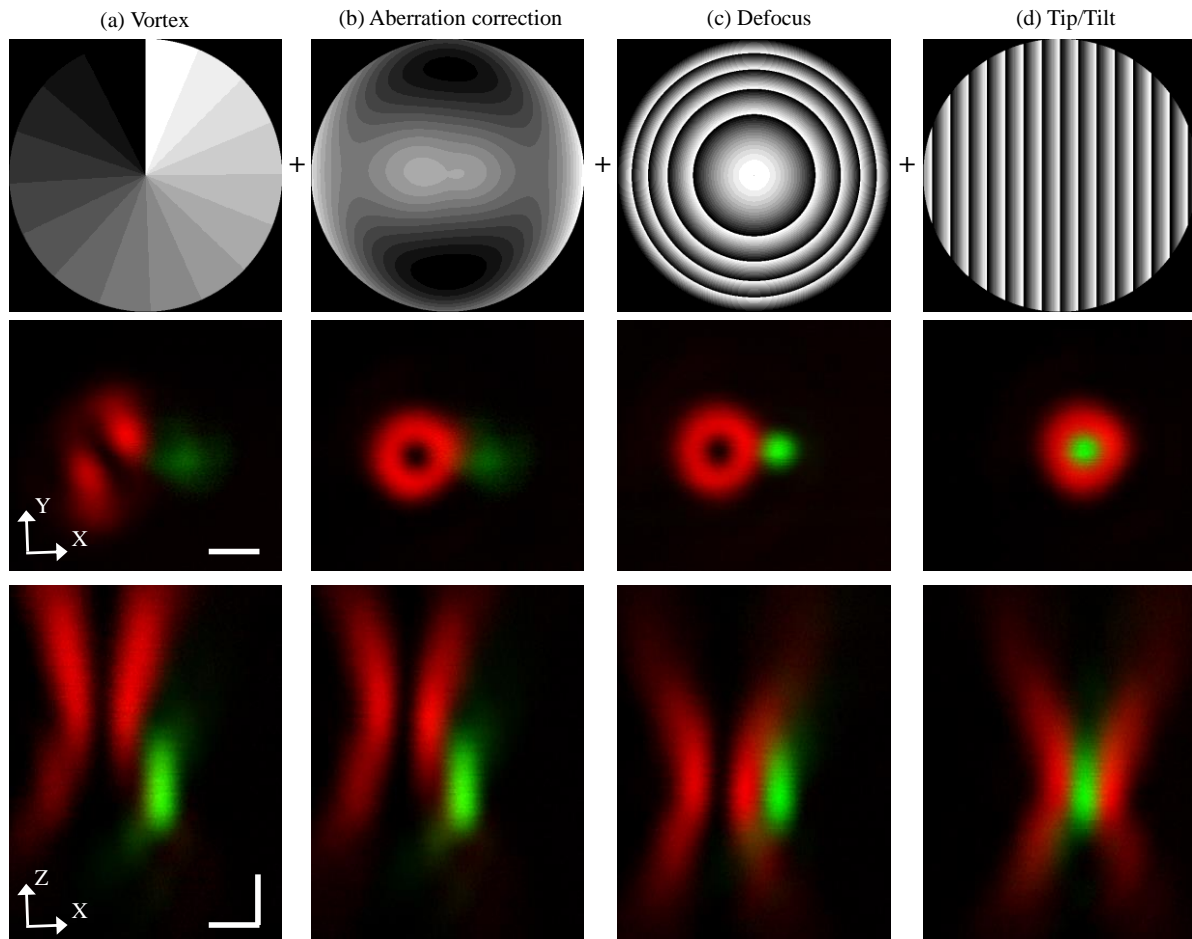


Figure 3. Use of a spatial light modulator for STED microscopy. (a-d) Measurement of the excitation and depletion point spread functions at the focus of a 100x/1.4NA oil immersion objective lens for various phases applied on the spatial light modulator. (a) A radial phase ramp from 0 to 2π is applied on the spatial light modulator. (b) Optical aberrations introduced by the optical set up are compensated by introducing various coefficients of Zernike aberration modes. (c,d) Adjustment of the axial and lateral spatial overlap between the excitation and depletion beams by introducing various amounts of defocus and tip/tilt modes. Scale bars: 500nm.

2.4 Rigorous estimation of the STED spatial resolution

The spatial resolution of our STED microscope was estimated from images of fluorescent beads of a 20 nm diameter (20 nm Crimson beads, Invitrogen) for gradual depletion intensities (Figure 4). Isolated beads were found automatically and fitted individually with 2D Gaussian function using custom Matlab scripts (Matlab, Mathworks). By using this procedure for each depletion intensity and over a large population of beads ($N=200-300$) we obtained a histogram of the full-width-half maximum of the point spread function from the 20 nm beads. The spatial resolution of the microscope was then estimated as the mean value of each histogram. This was obtained by fitting each histogram with a 1D Gaussian distribution and with a confidence interval at 68 %, estimated from the variance of the Gaussian distribution.

The fluorescent beads were diluted and attached to a microscope coverslip coated with Poly-L-lysine and embedded in 2,2'-Thiodiethanol³⁶ (TDE mounting medium, Aberriors). The following acquisition parameters were used for imaging: $20 \times 20 \mu\text{m}^2$ field of view, 20 nm pixel size and 30 μs pixel dwell time. The maximum peak intensity of the depletion beam at the focus of the objective was estimated using the following relation³⁷:

$$\frac{2P_{\text{STED}}}{e \times \pi \omega^2} \times \frac{T_{\text{Rep}}}{\tau_{\text{STED}}} \times T, \quad (4)$$

where P_{STED} is the average power of the depletion beam at the back aperture of the microscope objective, ω_{STED} is a parameter related to the spatial extend of the depletion beam, T_{Rep} is the repetition rate of the Ti:S laser, τ_{STED} is the pulse duration of the depletion beam, and T the transmission of the microscope objective lens at $\lambda = 765 \text{ nm}$ (See Table 2 for different parameters values).

Table 2. Parameters used to estimate the depletion intensity at the focus of the microscope objective

Parameters	$P_{\text{STED MAX}}$	ω_{STED}	T_{Rep}	τ_{STED}	T
Values	39 mW	350 nm	12.5 ns	100 ps	70 %

When no depletion beam is applied, the spatial resolution of the STED microscope, which corresponds to the confocal resolution, is $270 \pm 20 \text{ nm}$. As expected in the presence of a depletion hollow beam at $\lambda = 765 \text{ nm}$ the spatial resolution decreases with the depletion intensity and our results are in good agreement with the expected values obtained from equation (3). Currently, the spatial resolution of our STED microscope is $82 \pm 14 \text{ nm}$, for a depletion peak intensity of 650 MW/cm^2 . This corresponds to an improvement by a factor of 3.3 and we note that the resolution of our microscope is certainly limited by the amount of light still present at the “null” of the depletion beam, which is approximately 5–7 % of the maximum intensity.

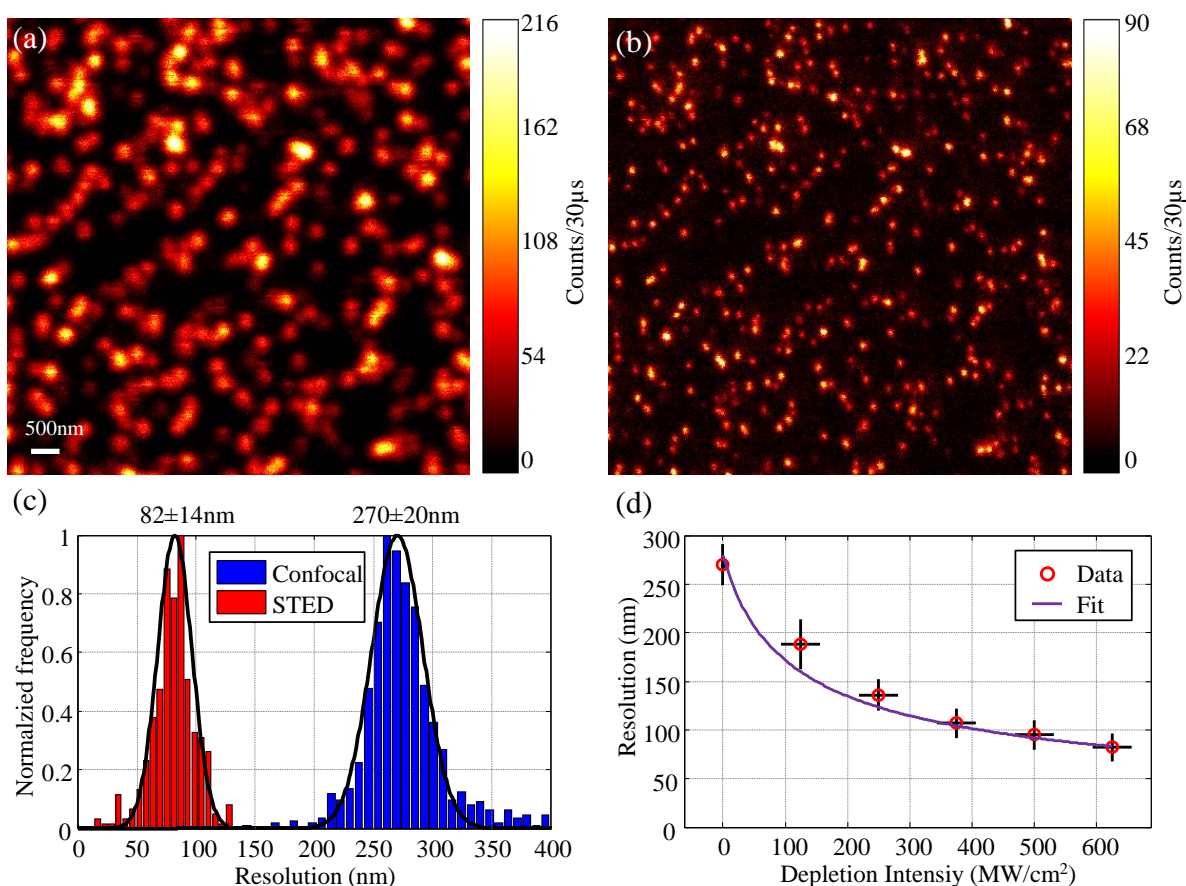


Figure 4. Characterization of the spatial resolution with fluorescent beads. (a,b) STED and confocal images of 20 nm fluorescent beads. (c,d) Estimation of the confocal and STED resolution as function of the depletion peak intensity. Scale bar, 500 nm.

3. SUPER-RESOLUTION IMAGING OF AMYLOID FIBRILS

3.1 Aggregation and labelling of the α -synuclein proteins

Fibrils were formed by incubating seed fibrils and monomers of the human protein α -synuclein in 50 mM sodium phosphate buffer at pH 7.4 for 48h at 37°C. The seed fibrils and monomers were prepared according to the protocols detailed in¹⁰ and diluted to a final concentration of 2 μ M and 20 μ M respectively. After 48 h longer fibrils are formed due to the addition of monomeric protein. They were then drop-casted onto a microscope coverslip of a Labtek chambered well, previously coated with poly-L-lysine. Labelling of the fibrils was done by standard immunofluorescence staining. The fibrils were first incubated for 1 h with blocking buffer (goat serum diluted at 5 % in 50 mM sodium phosphate buffer at pH 7.4). The fibrils were then incubated for 1 h with a primary mouse antibody against α -synuclein (α -Synuclein Mouse mAb LB509, Life technologies) and subsequently for another hour with an anti-mouse secondary antibody conjugated to the dye ATTO647N (Anti-Mouse IgG - Atto 647N, Sigma). Primary and secondary antibodies were diluted to a final concentration of 0.9 μ g/mL and 6 μ g/mL, respectively, in blocking buffer.

3.2 STED imaging of α -synuclein fibrils

STED imaging of α -synuclein fibrils labelled with the dye ATTO647N was performed with our custom-built microscope described and characterized in the previous sections. To avoid spherical aberration on the excitation and depletion beams, 2,2'-Thiodiethanol (TDE mounting medium, Aberrior) was added to the imaging well. The fibrils were imaged in field of view of up to 80 \times 80 μ m² using the acquisition parameters listed below, which correspond to a total acquisition time of up to 8 min per super-resolution image.

Table 3. Acquisition parameters for the STED imaging of α -synuclein fibrils

Parameters	P_{Exc}	P_{STED}	Field of view	Pixel size	Pixel dwell time
Values	80 μ W	39 mW	80 \times 80 μ m	20 nm	30 μ s

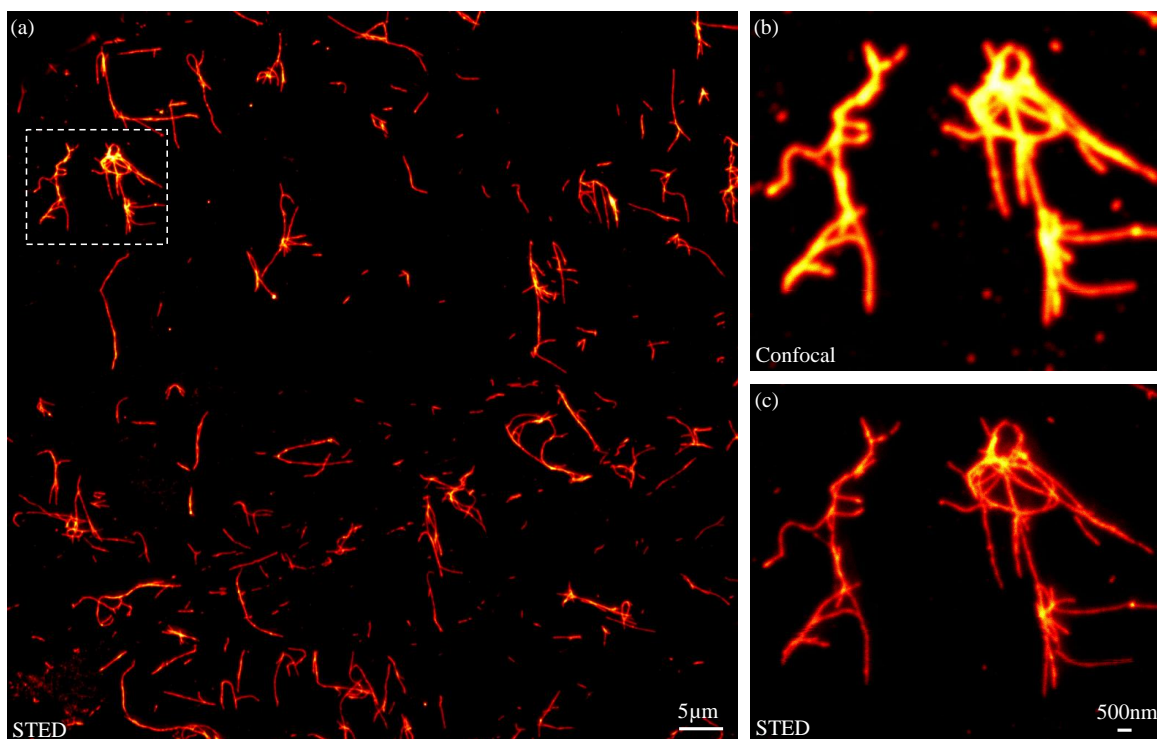


Figure 5. Super resolution imaging of α -synuclein fibrils labelled with ATTO647N using primary and secondary antibodies. (a) STED image recorded on a 80 \times 80 μ m² field of view with a 20 nm pixel size. Scale bar: 5 μ m. (b,c) STED and confocal enlarged images corresponding to the dashed box area. Scale bar: 500 nm.

4. CONCLUSION

In these proceedings we have reported on the implementation and application of a Stimulated Emission Depletion (STED) microscope to visualize amyloid fibrils *in vitro*. This home-built STED microscope is based on a supercontinuum source and a spatial light modulator. The former is a simple solution to excite various dyes, while the latter provides an effective way to generate aberration-free depletion patterns and to align routinely the excitation and depletion beams without moving any mechanical parts. Future work will focus on extracting quantitative parameters characterizing the amyloid fibril growth kinetics from the super-resolved images.

ACKNOWLEDGMENT

This work was supported by grants from the Leverhulme Trust, the Engineering and Physical Sciences Research Council, UK (grant EP/H018301/1), by the Medical Research Council (grant MR/K015850/1, and MR/K02292X/1), the Wellcome Trust (089703/Z/09/Z) and the Alzheimer Research UK Trust (ARUK-EG2012A-1). D.P. wishes to acknowledge support from the Swiss National Science Foundation and the Wellcome Trust with personal fellowships

BIBLIOGRAPHY

- [1] Selkoe, D. J., "Folding proteins in fatal ways," *Nature* **426**(6968), 900–904 (2003).
- [2] Jucker, M., Walker, L. C., "Self-propagation of pathogenic protein aggregates in neurodegenerative diseases," *Nature* **501**(7465), 45–51 (2013).
- [3] Fitzpatrick, A. W. P., Debelouchina, G. T., Bayro, M. J., Clare, D. K., Caporini, M. a., Bajaj, V. S., Jaroniec, C. P., Wang, L., Ladizhansky, V., et al., "Atomic structure and hierarchical assembly of a cross- β amyloid fibril," *Proc. Natl. Acad. Sci. U. S. A.* **110**(14), 5468–5473 (2013).
- [4] Kamihira, M., Naito, A., Tuzi, S., Nosaka, A. Y., Saitô, H., "Conformational transitions and fibrillation mechanism of human calcitonin as studied by high-resolution solid-state ^{13}C NMR," *Protein Sci.* **9**(5), 867–877 (2000).
- [5] Serpell, L. C., "Alzheimer's amyloid fibrils: structure and assembly," *Biochim. Biophys. Acta - Mol. Basis Dis.* **1502**(1), 16–30 (2000).
- [6] Milhiet, P. E., Yamamoto, D., Berthoumieu, O., Dosset, P., le Grimellec, C., Verdier, J. M., Marchal, S., Ando, T., "Deciphering the structure, growth and assembly of amyloid-like fibrils using high-speed atomic force microscopy," *PLoS One* **5**(10) (2010).
- [7] Khurana, R., Coleman, C., Ionescu-Zanetti, C., Carter, S. A., Krishna, V., Grover, R. K., Roy, R., Singh, S., "Mechanism of thioflavin T binding to amyloid fibrils," *J. Struct. Biol.* **151**(3), 229–238 (2005).
- [8] Andersen, C. B., Yagi, H., Manno, M., Martorana, V., Ban, T., Christiansen, G., Otzen, D. E., Goto, Y., Rischel, C., "Branching in amyloid fibril growth," *Biophys. J.* **96**(4), 1529–1536 (2009).
- [9] Ferkinghoff-Borg, J., Fonslet, J., Andersen, C. B., Krishna, S., Pigolotti, S., Yagi, H., Goto, Y., Otzen, D., Jensen, M. H., "Stop-and-go kinetics in amyloid fibrillation," *Phys. Rev. E - Stat. Nonlinear, Soft Matter Phys.* **82**(1) (2010).
- [10] Pinotsi, D., Buell, A. K., Galvagnion, C., Dobson, C. M., Kaminski Schierle, G. S., Kaminski, C. F., "Direct observation of heterogeneous amyloid fibril growth kinetics via two-color super-resolution microscopy," *Nano Lett.* **14**(1), 339–345 (2014).
- [11] Kaminski Schierle, G. S., Van De Linde, S., Erdelyi, M., Esbjörner, E. K., Klein, T., Rees, E., Bertoncini, C. W., Dobson, C. M., Sauer, M., et al., "In situ measurements of the formation and morphology of intracellular β -amyloid fibrils by super-resolution fluorescence imaging," *J. Am. Chem. Soc.* **133**(33), 12902–12905 (2011).

- [12] Hell, S. W., Wichmann, J., “Breaking the Diffraction Resolution Limit by Stimulated-Emission - Stimulated-Emission-Depletion Fluorescence Microscopy,” *Opt. Lett.* **19**(11), 780–782 (1994).
- [13] Rust, M., Bates, M., Zhuang, X., “Sub-diffraction-limit imaging by stochastic optical reconstruction microscopy (STORM),” *Nat. Methods* **3**, 793–796 (2006).
- [14] Betzig, E., Patterson, G. H., Sougrat, R., Lindwasser, O. W., Olenych, S., Bonifacino, J. S., Davidson, M. W., Lippincott-Schwartz, J., Hess, H. F., “Imaging intracellular fluorescent proteins at nanometer resolution,” *Science* (80-.). **313**(5793), 1642–1645, American Association for the Advancement of Science (2006).
- [15] Hess, S. T., Girirajan, T. P. K., Mason, M. D., “Ultra-high resolution imaging by fluorescence photoactivation localization microscopy,” *Biophys. J.* **91**(11), 4258–4272, Elsevier (2006).
- [16] Klar, T. A., Hell, S. W., “Subdiffraction resolution in far-field fluorescence microscopy,” *Opt. Lett.* **24**(14), 954–956 (1999).
- [17] Harke, B., Keller, J., Ullal, C. K., Westphal, V., Schönle, A., Hell, S. W., “Resolution scaling in STED microscopy,” *Opt. Express* **16**(6), 4154–4162 (2008).
- [18] Friedrich, M., Gan, Q., Ermolayev, V., Harms, G. S., “STED-SPIM: Stimulated emission depletion improves sheet illumination microscopy resolution,” *Biophys. J.* **100**(8) (2011).
- [19] Scheul, T., Wang, I., Vial, J.-C., “STED-SPIM made simple,” *Opt. Express* **22**(25), 30852–30864, Optical Society of America (2014).
- [20] Gould, T. J., Myers, J. R., Bewersdorf, J., “Total internal reflection STED microscopy,” *Opt. Express* **19**(14), 13351–13357 (2011).
- [21] Leutenegger, M., Ringemann, C., Lasser, T., Hell, S. W., Eggeling, C., “Fluorescence correlation spectroscopy with a total internal reflection fluorescence STED microscope (TIRF-STED-FCS),” *Opt. Express* **20**(5), 5243 (2012).
- [22] Bergermann, F., Alber, L., Sahl, S. J., Engelhardt, J., Hell, S. W., “2000-fold parallelized dual-color STED fluorescence nanoscopy,” *Opt. Express* **23**(1), 211, OSA (2015).
- [23] Pawley, J. B., “Handbook of Biological Confocal Microscopy, Second Edition,” *Opt. Eng.* **35**(9), 2765 (1996).
- [24] Willig, K. I., Harke, B., Medda, R., Hell, S. W., “STED microscopy with continuous wave beams,” *Nat. Methods* **4**(11), 915–918 (2007).
- [25] Wurm, C. A., Kolmakov, K., Göttfert, F., Ta, H., Bossi, M., Schill, H., Berning, S., Jakobs, S., Donnert, G., et al., “Novel red fluorophores with superior performance in STED microscopy,” *Opt. Nanoscopy* **1**(1), 7 (2012).
- [26] Morozova, K. S., Piatkevich, K. D., Gould, T. J., Zhang, J., Bewersdorf, J., Verkhusha, V. V., “Far-red fluorescent protein excitable with red lasers for flow cytometry and superresolution STED nanoscopy,” *Biophys. J.* **99**(2) (2010).
- [27] Bingen, P., Reuss, M., Engelhardt, J., Hell, S. W., “Parallelized STED fluorescence nanoscopy,” *Opt. Express* **19**(24), 23716 (2011).
- [28] Gould, T. J., Burke, D., Bewersdorf, J., Booth, M. J., “Adaptive optics enables 3D STED microscopy in aberrating specimens,” *Opt. Express* **20**(19), 20998 (2012).
- [29] Wildanger, D., Rittweger, E., Kastrup, L., Hell, S. W., “STED microscopy with a supercontinuum laser source,” *Opt. Express* **16**(13), 9614–9621 (2008).
- [30] Auksoorius, E., Boruah, B. R., Dunsby, C., Lanigan, P. M. P., Kennedy, G., Neil, M. A. A., French, P. M. W., “Stimulated emission depletion microscopy with a supercontinuum source and fluorescence lifetime imaging,” *Opt. Lett.* **33**(2), 113–115 (2008).
- [31] Bückers, J., Wildanger, D., Vicidomini, G., Kastrup, L., Hell, S. W., “Simultaneous multi-lifetime multi-color STED imaging for colocalization analyses,” *Opt. Express* **19**(4), 3130–3143 (2011).

- [32] Göttfert, F., Wurm, C. A., Mueller, V., Berning, S., Cordes, V. C., Honigmann, A., Hell, S. W., “Coaligned dual-channel STED nanoscopy and molecular diffusion analysis at 20 nm resolution,” *Biophys. J.* **105**(1) (2013).
- [33] Deng, S., Liu, L., Cheng, Y., Li, R., Xu, Z., “Effects of primary aberrations on the fluorescence depletion patterns of STED microscopy,” *Opt. Express* **18**(2), 1657–1666 (2010).
- [34] Donnert, G., Keller, J., Medda, R., Andrei, M. A., Rizzoli, S. O., Lührmann, R., Jahn, R., Eggeling, C., Hell, S. W., “Macromolecular-scale resolution in biological fluorescence microscopy,” *Proc. Natl. Acad. Sci. U. S. A.* **103**(31), 11440–11445 (2006).
- [35] Deng, S., Liu, L., Cheng, Y., Li, R., Xu, Z., “Investigation of the influence of the aberration induced by a plane interface on STED microscopy,” *Opt. Express* **17**(3), 1714, OSA (2009).
- [36] Staudt, T., Lang, M. C., Medda, R., Engelhardt, J., Hell, S. W., “2,2'-thiodiethanol: a new water soluble mounting medium for high resolution optical microscopy,” *Microsc. Res. Tech.* **70**(1), 1–9 (2007).
- [37] Moffitt, J. R., Osseforth, C., Michaelis, J., “Time-gating improves the spatial resolution of STED microscopy,” *Opt. Express* **19**(5), 4242–4254 (2011).